Accepted Manuscript

Experimental Investigation of the Aeroacoustics of Synthetic Jet Actuators in Quiescent Conditions

Jonne Jeyalingam[a], Mark Jabbal[b,*]

[a] *College of Engineering, Design and Physical Sciences, Brunel University London, UB8 3PH, UK*
[b] *Faculty of Engineering, University of Nottingham, NG7 2RD, UK*

[*] Corresponding author. Tel: +44 (0)115 951 4096; E-mail address: mark_jabbal@hotmail.com

Highlights

- Jet noise of a synthetic jet actuator is isolated from its diaphragm noise to assess aeroacoustic characteristics
- The actuator aeroacoustic response, in the form of audible whistling, is found to occur in a similar Strouhal number range as other pipe and orifice flow systems
- A threshold in the jet Reynolds number is established for the onset of flow-induced sound
- Good agreement between the acoustic spectra, velocity spectra and Schlieren visualisation of the synthetic jet

Abstract

In this paper, the aeroacoustic characteristics of a circular orifice, synthetic jet actuator in quiescent conditions is investigated. Electromagnetic actuation, in the form of a shaker-driven actuator with latex diaphragm, proved to be desirable over piezoelectric actuation for this work due to the reduced diaphragm noise contribution to overall actuator self-noise, hence making it easier to identify jet-related noise. Acoustic and velocity data, collected from microphone measurements in an anechoic chamber and hotwire measurements respectively, were compared for correlation. Schlieren visualization was also used to show synthetic jet development near the orifice. Flow-induced sound in the form of an audible whistling was found to occur for a Strouhal number range of $0.24 < St < 0.50$. A threshold in the jet Reynolds number of $600 < Re_j < 750$ was established for the onset of whistling from the actuator for all drive voltages. Coherence between the acoustic spectra and velocity power spectra is shown, with evidence of a feedback mechanism consisting of vortices shed at a frequency that coincides with acoustic modes of the actuator.

Keywords

Synthetic jet actuator; aeroacoustics; Pfeifentone; whistling; noise

1. Introduction

Synthetic jet actuators (SJAs) use an oscillating diaphragm to displace small volumes of air within a cavity to generate periodic jets that enter and exit the cavity through an orifice. These jets formed at the orifice, composed of vortex structures, have potential to be applied in the delay of flow separation on aircraft [1]. To minimise actuator size and weight, piezoelectric diaphragms, such as ones made of a lead zirconate titanate (PZT) patch bonded to a thin brass substructure, can be used instead of larger and heavier electromagnetic actuators [2,3]. In previous work that use active flow control to reduce flow-generated noise it was found that although the flow-generated noise source can be attenuated, the actuator self-noise outweighs any acoustic benefits [4-6]. The need to reduce SJA self-noise to make these devices viable for consideration in commercial applications is prevalent.

For a SJA, regardless of the actuation method used, there is a mass displacement of air during its operation and it can therefore treated as a monopole acoustic source that represents a pulsating sphere [5]. Sound generated by turbulence in an unbound flow, such as a synthetic jet, is generally referred to as aerodynamic sound [7]. Turbulence typically occurs in motion of fluid over a surface or due to flow instabilities, where a very small fraction of the rotational kinetic energy of the flow results in acoustic radiation. Lighthill discusses the mechanism behind aerodynamic sound that is produced as a by-product of airflow [8]. In jets emanating from a pipe-orifice system, instabilities in the jet flow cause periodic vortex shedding. If the time scale of these vortices matches an

acoustic scale of the system, these are excited and amplified causing self-sustained periodic oscillations [9]. These oscillations are the source of a whistling noise, also known as Pfeifentone.

Arik [10] recorded noise levels reaching 73 dB for a piezoelectrical-driven SJA and was able to reduce self-noise to 30 dB using a muffler system. More recently, Bhapkar et al. [11] showed that reducing the orifice diameter can reduce can result in lowering overall noise levels of an electromagnetic-driven SJA by up to 17%. This is expected since, with increasing orifice diameter, the mass associated with the orifice increases and leads to higher noise levels. Bhapkar et al. [12] showed that a smaller orifice height and can reduce the sound pressure level generated by a SJA by up to 10%.

The focus of this paper is to better understand and define the operating parameters of a circular orifice SJA that generates aerodynamic noise in quiescent conditions. The work considers actuator self-noise, particularly the aeroacoustic response, and the operating conditions that lead to flow-induced sound. A better understanding will help establish operating parameters for optimal SJA operation with minimal self-noise generation.

Peak velocity performance of a SJA is achieved by operating the device at the synthetic jet resonant frequency, which closely coincides with the mechanical resonance frequency. However, due to the inherent "noisy" acoustic spectrum of commercial piezoceramic diaphragms associated with the presence of several harmonic frequencies of the actuation frequency, f_a, it is difficult to distinguish jet noise from the diaphragm noise [13]. For this reason, electromagnetic actuation with a latex membrane for the SJA diaphragm was chosen to study the effect of jet noise without the excessive influence of diaphragm noise in the acoustic data (Fig. 1). A vibration generator that oscillates a latex membrane at lower frequencies (below 100 Hz) to generate synthetic jets is used for this purpose. The acoustic spectrum for this is much smoother and makes it easier to differentiate from jet noise.

Acoustic spectra obtained can then be compared to power spectral density (PSD) calculated from the jet velocity data for coherence. To understand the relationship between jet noise and SJA operating conditions, the two fundamental, non-dimensional jet parameters of synthetic jets in quiescent conditions are to be considered. These are the jet Reynolds number, Re_j, and stroke length, L [14]. Re_j is defined according to Eq. (1)

$$\mathrm{Re}_j = \frac{\overline{U}_0 d}{\nu} \tag{1}$$

Where d is the SJA orifice diameter, ν the dynamic viscosity and $\overline{U}_0$ is the time averaged blowing velocity over the full cycle, as defined by Smith and Glezer [15], and is represented by Eq. (2)

$$\overline{U}_0 = \frac{1}{T} \int_0^{T/2} \tilde{u}_0(t) dt \tag{2}$$

Where $\tilde{u}_0$ is the space-averaged instantaneous jet velocity, and T is the period of the actuation cycle. The stroke length, L, is defined as the non-dimensional length of the air column expelled through the orifice during the blowing phase, L_0, as shown in Eq. (3)

$$L = \frac{L_0}{d} = \frac{\overline{U}_0}{fd} \tag{3}$$

2. Experimental Approach

The objective of the experiment is to gain a better understanding of the aeroacoustic response of a SJA. The actuator used in the experiments has a tensioned latex membrane clamped in place of a PZT diaphragm (Fig. 2a). The actuator was originally designed to be driven by a 50 mm diameter PZT diaphragm, giving a cavity diameter of 48 mm. The diaphragm is connected to a vibration generator via a shaft and a thin brass plate (27 mm diameter) acts as a bonding surface between the membrane and the shaft. The actuator has an orifice with diameter, d, 2 mm and height, h, 4.2 mm and a cavity of height, H, 1.2 mm. This geometry ($h/d = 2.1$ and $H/D = 0.6$) was chosen based on the peak jet velocity optimised SJA configuration [16]. The SJA was set up on a compound table for hot wire anemometry measurements of the jet velocity (Fig. 2b).

A Dantec hotwire anemometry system with a single-sensor 55P11 hotwire probe is used to measure the jet velocity at various positions relative to the orifice exit plane. The sampling frequency was set to 10 kHz and the number of samples was 60,000. For frequency response measurements of the SJA, the probe was fixed centrally at approximately $1d$ from the orifice exit. To acquire data for the power spectral densities at various locations within the jet, the probe was traversed vertically in the streamwise direction to $20d$ at equal intervals of $5d$ from the orifice exit, and in the spanwise direction between 0-$2d$. The percentage error in the velocity measurement using hot wire anemometry is 3%. In addition, a Microtrak 3 system laser displacement sensor is used to measure

the diaphragm peak-to-peak displacement for the different cases (Fig. 2b). The measurement system uses a sampling frequency of 300 Hz with measurement errors of +/- 4 μm, equating to +/- 0.4%.

SJA noise tests were conducted in a purpose built, hemi-anechoic chamber to facilitate aeroacoustic measurements [17]. A ½" PCB 426E01 condenser microphone, placed 40d from the jet exit at a grazing incidence of 30° to the orifice, is used (Fig. 2c). According to Viswanathan [18], it is preferable to position the microphone at least 35d away for true far field noise measurements. This distance is similar to the guidelines by Ahuja [19], where a distance of 40-72d is suggested for far field jet measurements. Microphone sensitivity is +/- 1.5 dB, equating to a measurement error of +/- 4%.

The test setup for Schlieren visualization of the synthetic jet is shown in Fig. 2d. A white LED light source emits light that is reflected by a parabolic mirror placed behind the SJA. The light travels through carbon dioxide gas, which is introduced near the SJA orifice plate to be entrained by the ensuing jet and is refracted. A knife edge is placed in such a way as to focus and partially obstruct the reflected and refracted light to form the shadow. A high-speed camera with a telephoto lens and resolution of 1280 by 720 pixels was used to capture image sequences at a frame rate of 1000 fps.

The acoustic response of the SJA is comprised of the vibration generator, which becomes more dominant after f_a = 80 Hz with decreasing jet velocity, and the oscillating jet expelled through the orifice. To separate the two noise sources, measurements of the actuator with and without the orifice plate (SPL$_{overall}$ and SPL$_{diaphragm}$, respectively) were taken to obtain ΔSPL according to Eq. (4).

$$\Delta SPL = SPL_{overall} - SPL_{diaphragm} \tag{4}$$

Measurements of just the vibration generator noise (and small noise contributions that may originate from the diaphragm and possible vibrations associated to the system), SPL$_{diaphragm}$, is subtracted from the noise of the SJA operating with the orifice plate, SPL$_{Overall}$, where the remaining noise can be attributed to aeroacoustic noise, ΔSPL. Although this does not guarantee full isolation of the aeroacoustic noise from the vibration generator and diaphragm, it helps minimise their contribution to the acoustic spectrum.

Three test cases are considered which differ in peak sinusoidal voltage input to the diaphragm: Case 1 (3 V), Case 2 (4 V) and Case 3 (5 V) across actuation frequencies, f_a, of 5-90 Hz. The acoustic spectra is presented and compared with the velocity spectra (in the form of Re$_j$, L and PSD) derived from the hotwire velocity data to establish correlation between the two datasets.

3. Results

3.1 Frequency Response

Fig. 3 shows the SJA frequency response in terms of diaphragm peak-to-peak displacement (Fig. 3a) and peak jet velocity (Fig. 3b). It is interesting to note that the actuation frequency for peak jet velocity does not coincide with the maximum diaphragm displacement, which is associated with the largest change in cavity volume. Peak jet velocity is measured at 55 Hz (Case 1) and 60 Hz (Case 2 and 3), whereas maximum displacement is measured at 45 Hz for all cases. Furthermore, the diaphragm peak-to-peak displacement shows linear proportionality to the input voltage (Fig. 3a), whereas the gain in peak jet velocity becomes smaller with increasing voltage input (Fig. 3b).

3.2 Acoustic Spectra

Fig. 4 shows the acoustic spectra for all three input cases. At low actuation frequencies and jet velocities, the resulting sound pressure level, ΔSPL, remains around zero until a sudden spike between 2 and 5 kHz. For Case 1 (Fig. 4a) this spike in self-noise is first recorded at 3781 Hz at an actuation frequency of 35 Hz, corresponding to a jet velocity of 18.2 m/s. For Case 2 and 3, the spike occurs at actuation frequencies of 20 Hz (15.4 m/s) and 15 Hz (18.3 m/s) respectively (Figs. 4b and 4c). Distinct patterns are evident in the spectra, which can help identify possible noise sources. These are constant frequency lines and a bow like pattern seen at higher frequencies above 3781 Hz. Constant frequency lines in the spectrum, such as the one originating from around 2879 Hz (f_1), and 3781 Hz (f_2), indicates an acoustic mode of the SJA system. The frequencies associated with the bow line branching off f_2 have a constant Strouhal number, St, as discussed further in Section 3.2.1, and are denoted by f_{St}. In all cases, the length of the bow coincides with the envelope for whistling (marked by dash black lines), while the peak in the bow coincides with the peak jet velocity (marked by the dash white line). In addition to these fundamental frequencies, f_1 and f_2, their subharmonics and higher harmonics are increasingly visible with increasing input voltage.

3.2.1 Strouhal number dependence

In various literature it has been established that the whistling in pipe systems and jets emanating from an orifice are related to flow instabilities that occur within a specific Strouhal number, St, range based on the fundamental frequency as shown in Eq. (5).

$$St = \frac{fd}{U} \tag{5}$$

Arthurs and Ziada [20] found $0.26<St<0.56$ for an annular duct with closed coaxial side-branches to cause resonance. Henrywood and Agarwal [21] recorded $0.2<St<0.6$, which is indicative of vortex shedding due to jet instabilities [22]. Using Eq. (5) the calculated Strouhal number, based on f_2 (the most dominant frequency in the spectrum) and the jet exit velocity, is $St = 0.22$ for Case 1 at an actuation frequency of 60 Hz. In fact, the Strouhal numbers for jet velocities associated with the different acoustic modes, f_1 and f_2, seen in the spectra for all cases fall within the range $0.22<St<0.50$, as shown in Fig. 5a, and are thus in close agreement with the literature. Fig. 5a shows St as a function of jet velocity, where the red region marks the constant frequency lines on the acoustic spectra. This is indicative of acoustic modes of the SJA system. On the other hand, the bow-like SPL peak lines in the spectra branching off from f_2 cannot be attributed to the SJA geometry and therefore not caused by acoustic modes of the cavity and/or orifice. When Strouhal numbers of the frequencies at which the SPL peaks form the bow pattern (i.e. f_{St} in Fig. 4) are plotted against actuation frequency, a distinct constant St trend can be seen (Fig. 5b). For Case 1, this is between $f_a \cong 35$-80 Hz, Case 2 between $f_a \cong 30$-75 Hz and Case 3 between $f_a \cong 25$-90 Hz.

3.2.2 Reynolds number dependence

The jet Reynolds number, Re_j, defined in Eq. (1) is shown as a function of actuation frequency for all cases in Fig. 6a. The variable is $\overline{U}_0$, but presented as Re_j allows for universal identification of SJA operating conditions that result in the generation of jet noise. When compared to the acoustic spectra (Fig. 4) specific self-noise conditions related to Re_j become evident. For all cases, a threshold range for Re_j exists, $624< Re_j<742$, within which whistling noise contributes to the actuator self-noise (as marked by the dash lines). When compared to the acoustic spectra for Case 1 (Fig. 4a), ΔSPL at $f_a = 90$ Hz has diminished to near zero above 1 kHz. Although acoustic and velocity measurements were not taken beyond $f = 90$ Hz, similar trends are observed with the other two cases, where ΔSPL approaches zero at $Re_j \cong 650$.

Furthermore, for an actuation frequency of 40-45 Hz there is a shift in high frequency noise branching from f_1 towards higher frequencies, which appears as a bow in the spectrum. This is clearly Re_j dependent, as the shift increases with increasing Re_j until a peak is reached that coincides with peak jet velocity. For example, the maximum shift for Case 1 is reached at $f = 55$ Hz, after which the shift decreases again until merging back together with the mode it branched off from. This, together with the constant St behaviour and frequency shift, is indicative of a second noise source likely due to jet instabilities and more aggressive breakup of flow structures that results in increased turbulent mixing further downstream with increasing jet velocity. Similar observations in the same St range were noted by Henrywood and Agarwal [21].

3.2.3 Stroke length dependence

The non-dimensional stroke length, L, defined in Eq. (3) is shown as a function of actuation frequency for all cases in Fig. 6b. Again, the only variable that changes for L in this case is $\overline{U}_0$. A noticeable trend for all cases is a sudden jump in L, marked by the dash lines. It was shown in Fig. 4 that these actuation frequencies roughly correspond to the onset of actuator self-noise. For example, for Case 1 this jump takes place at $f_a = 35$ Hz, the same actuation frequency where whistling noise is first measured. This could be explained as the effect of onset of jet instabilities and vortex shedding that results in generating whistling noise once a threshold Re_j is reached.

3.3 Velocity Spectra and Schlieren Visualisation

According to the literature, flow instabilities and vortex shedding have been linked to the excitation of the cavity-orifice system at their fundamental modes. Evidence of this is observed in the acoustic spectra in the form of constant frequency lines that occur within a specific range of Strouhal numbers typical of such noise mechanism. Self-sustained oscillations in the flow cause turbulence and periodic whistling noise if the jet meets the right conditions for Re_j and St. The jump in L (Fig. 6b) is related to the highly fluctuating and changing velocity of the transitioned, turbulent jet. The Strouhal number analysis indicates the self-noise source to be related to self-sustained periodic oscillations caused by growing jet instabilities and vortex shedding, which should be detectable in the hotwire data and Schlieren visualisation.

4

Fig. 7 shows the instantaneous jet velocity response for all cases. At actuation frequencies below which the acoustic spectra show a mean $\Delta SPL \cong 0$, the velocity response is smooth with no fluctuations. This is visible for Case 1 (Fig. 7a), where for $f_a = 25$ Hz and 30 Hz, smooth responses are observed. However at and beyond the onset of whistling, ($f_a = 35$ Hz and 40 Hz respectively), increased fluctuations are seen in the velocity responses. Specifically, the onset of fluctuations are seen near the velocity peaks, corresponding to the end of the blowing part of the SJA cycle (e.g. $t \cong 0.02$ s) and after which the jet becomes unstable and transitions to turbulence. From Fig. 4a the actuator self-noise starts to rapidly decrease at and beyond $f_a = 80$ Hz, and accordingly the velocity responses for $f_a = 80$ and 85 Hz are relatively smooth compared with those at $f_a = 60$ and 75 Hz (Fig. 7b). A similar behaviour is observed in Cases 2 and 3. In Case 2, a smooth velocity response is evident before the onset of whistling ($f_a = 20$ Hz, Fig. 7c) followed by signal fluctuations marking jet transition to turbulence ($f_a = 25$ Hz, Fig. 7c). In Case 3 (Fig. 4c) there is a range of actuation frequencies between $f_a = 60\text{-}80$ Hz where the SPL decreases at the dominant frequencies, f_1, f_2 and f_{St}. Similarly, fluctuations in the velocity response also decrease at $f_a = 60$ Hz (Fig. 7d).

A visual representation of these findings is shown in Fig. 8 in the form of Schlieren visualisation. Case 2 is used for comparison as the beginning and end of the constant frequency characteristics are fully visible in the acoustic spectrum. At an actuation frequency $f_a = 20$ Hz, a laminar jet forms at the exit with some initial vortex roll up (Fig. 8a). The vortex pair formed is weak and elongated (t = 0.08T) as it quickly moves downstream with the jet flow before breaking up relatively early at t = 0.22T (7d) to form a turbulent jet. The point of transition to turbulence is pushed further downstream and reaches its furthest point at 9d from the orifice exit, which is also at the end of the blowing part of the cycle (t = 0.48T) with a peak centreline velocity of 15.4 m/s. Once the diaphragm starts moving in the opposite direction for the suction part of the cycle, the jet slows down and dissipates. Increasing the actuation frequency to $f_a = 25$ Hz marks the onset of the periodic whistling noise for Case 2 (Fig. 4b). Similar to the previous case of $f_a = 20$ Hz, a laminar jet clearly forms at the orifice exit (Fig. 8b), which breaks up around 8d. The transition point is again pushed further downstream (10d) as more air exits the orifice (t = 0.28T). However, as the diaphragm moves back in the opposite direction, initiating the suction cycle, the transition point begins to move upstream towards the orifice until the entire jet becomes fully turbulent (t = 0.33T). At this point, shear layers are visible on either side of the fully turbulent jet. A closer look at the shear layer at t = 0.45T reveals small periodic flow structures within it. These structures are the result of periodic vortex shedding caused by excitation of the SJA system at an acoustic mode, which in turn induces and amplifies vortex shedding near the orifice exit. Finally, Fig. 8c shows the jet development for $f_a = 60$ Hz where the highest jet velocity of 30 m/s is measured. The jet is again initially laminar, however between t = 0.27T and t = 0.33T it becomes turbulent within 1d from the orifice exit. From the acoustic spectra in Fig. 4b, the SPL level of f_2 is about the same at $f_a = 60$ Hz and $f_a = 25$ Hz, but a key difference is the high frequency noise that appears as a bow in the spectrum.

The Schlieren images and velocity plots show a clear relationship between the actuator self-noise generation and turbulent jet flow. However, at this stage it is not known if the vortex shedding frequencies indeed match the system resonance frequencies. For this, the frequency components that make up the jet velocity signal (PSD) can be analysed to establish if coherence between the acoustic and velocity spectra exists. Fig. 9 shows the velocity PSD spectra for Case 2 while generating its peak jet velocity at $f_a = 60$ Hz. At the centre of the orifice (Fig. 9a) there is an increase in the spectral band in the low to mid-frequency range from the exit to a downstream distance of y=10d, which suggests the formation of the jet [15]. With increasing distance downstream from the orifice, the low frequency peaks are quickly attenuated. This attenuation leaves a continuous spectrum, characteristic of turbulence, which indicates the existence of eddies of various sizes [23]. In the spanwise direction, between x/d = 0 and 0.5 at the exit (Fig. 9a and 9b respectively), the magnitude of low frequency band increases slightly, suggesting the development of the jet.

Moving along the spanwise direction at y=5d, there is no change in the spectrum until x=1d (Fig. 9c), where an increase in high frequency components is seen. This region is located just outside the orifice where it was shown, in Schlieren images (t = 0.33T, Fig. 8c), a turbulent shear layer develops at $f_a = 60$ Hz with periodic small-scale flow structures occurring. Also, as the jet spreads in the spanwise direction, the large-scale structures continue to dissipate as they transfer their energy to the smaller scales, evidenced by the dissipation of low frequency components slowly and the gain or slower decrease of high frequency components, slowly becoming a continuous spectrum. This is due to the spanwise spread of the jet and flow structures and shows that some of the small-scale structures maintain their energy as they move downstream, while the large-scale structures continue to dissipate as they transfer their energy to the smaller scales. In Fig. 9d the spectra at the exit and y=5d positions contain very little energy because these lie outside the main influential region of the jet of the low spreading rate of the jet.

5

As the noise radiation from the jet is a result of flow structures formed in the separating shear layer from the orifice (which, under the right conditions, can also excite and amplify acoustic modes of the SJA) and energy dissipation from turbulence, it is now possible to compare acoustic and velocity spectra for coherence. Fig. 10 compares the velocity and acoustic spectra for Case 2. In this comparison the velocity spectrum shown in Fig. 9c is chosen as the variation in energy across the spectrum, especially at y=5d, shows excellent agreement with the acoustic spectrum. This chosen point for this comparison is located in the jet shear layer, where most of the jet noise sources originate from. However, it also must be said that not all noise contributions are explained by the velocity spectrum. Equally not all peaks in the velocity spectrum can be linked to the jet related noise. This is mainly due to hot wire rectification [15,24], a source of error that needs to be considered when using a 1D probe that does not take the flow direction into account.

Conclusions

The aeroacoustic characteristics of a synthetic jet actuator (SJA) with circular orifice was investigated in quiescent conditions. Electromagnetic actuation, in the form of a shaker-driven SJA, proved to be desirable over piezoelectric actuation for this work due to the reduced diaphragm noise contribution to overall actuator self-noise, hence making it easier to identify jet-related noise. The experimental work consisted of hot-wire anemometry and microphone recordings to conduct velocity and acoustic spectra measurements respectively across a range of actuation frequencies (5-90 Hz) and SJA peak drive voltages (3, 4 and 5 V). Schlieren visualisation was also used to show the behaviour of the synthetic jet flow structures.

Key findings from the experimental work are as follows:

1. It was shown that the SJA aeroacoustic response is dictated by a Strouhal number range of 0.22<St<0.50, which corroborates values recorded for other orifice and pipe flow systems. When vortices from the jet are shed at a frequency that matches an acoustic mode of the actuator, a feedback mechanism is established that generates a self-sustained tone, Pfeifentone or whistling, through the blowing portion of the actuation cycle.
2. A threshold in the jet Reynolds number, Re_j, of 600<Re_j<750 was established for the onset of whistling from the SJA for all drive voltages.
3. The non-dimensional stroke length, L, shows a sudden increase at or near the actuation frequency related to the onset of whistling. Schlieren visualisation shows that this increase is related to jet instabilities and vortex shedding that occur after this point.
4. There is good agreement when comparing the acoustic spectra to the velocity spectra of corresponding SJA drive voltages. An increase in energy seen at specific higher frequencies in the velocity spectra match those of resonance modes seen in the acoustic spectra. This increase is evidence of a feedback mechanism.

This work offers an improved understanding of the aeroacoustic response of an electromagnetic-driven SJA in quiescent conditions and the dimensionless jet flow parameters that cause flow-induced sound. A better understanding will help establish operating parameters for optimal SJA operation with minimal self-noise generation. Further work is required to compare different actuation methods, including piezoelectric, to confirm similar conditions apply and what additional contributions there may be from sources such as turbulent mixing noise from higher velocity jets.

Acknowledgements

References

[1] M. Jabbal, S. Liddle, J. Potts, W. Crowther, Development of design methodology for a synthetic jet actuator array for flow separation control applications, Proc. IMechE. Part G: J. Aerosp. Eng. 227 (2013) 110-124.

[2] J. S. Agashe, M. Sheplak, D. P. Arnold, L. N. Cattafesta, MEMS-based actuators for flow-control applications, IUTAM Symp. Flow Control MEMS 7 (2008) 25-32.

[3] D. C. McCormick, Boundary layer separation control with directed synthetic jets, Proc. 38th AIAA Aerosp. Sci. Meet. Exhib., AIAA 2000-0519, Reno, NV, 10-13 January 2000.

[4] J. H. Kim, L. Al-Sadawi, A. Vathylakis, T. P. Chong, Trailing edge noise reduction by passive and active flow controls, Proc. 20th AIAA/CEAS Aeroacoust. Conf., AIAA 2014-3300, Atlanta, GA, 16-20 June 2014.

[5] W. Devenport, S. Glegg, Fundamentals and Applications of Modern Flow Control, first ed., AIAA, Reston, 2008, 353-372.

[6] C. E. Seeley, M. Arik, R. Hedeen, Y. Utturkar, T. Wetzel, M.-Y. Shih, Coupled acoustic and heat transfer modeling of a synthetic jet, Proc. 47th AIAA/ASME/ASCE/AHS/ASC Struct., Struct. Dynamics Mater. Conf., AIAA 2006-1879, Newport, RI, 1-4 May 2006.

[7] M. S. Howe, Theory of Vortex Sound, Cambridge University Press, 2003.

[8] M. J. Lighthill, On sound generated aerodynamically I. General theory, Royal Soc. London. Series A, Math. Phys. Sci. 211 (1952) 564-587.

[9] V. Nair, R. Sujith, Precursors to self-sustained oscillations in aeroacoustic systems, Intl. J. Aeroacoust. 15 (2016) 312-323.

[10] M. Arik, An investigation into feasibility of impingement heat transfer and acoustic abatement of meso scale synthetic jets, Appl. Therm. Eng. 27 (2007) 1483-1494.

[11] U. Bhapkar, A. Srivastava, A. Agrawal, Acoustic and heat transfer aspects of an inclined impinging synthetic jet, Appl. Intl. J. Them. Sci. 74 (2013) 145-155.

[12] U. Bhapkar, A. Srivastava, A. Agrawal, Acoustic and heat transfer characteristics of an impinging elliptical synthetic jet generated by acoustic actuator, Intl. J. Heat Mass Transfer 79 (2014) 12-23.

[13] J. Jeyalingam, M. Jabbal, Optimization of synthetic jet actuator design for noise reduction and velocity enhancement, Proc. 8th AIAA Flow Control Conf., AIAA 2016-4236, Washington, D.C., 13-17 June 2016.

[14] A. Glezer, The formation of vortex rings, Phys. Fluids 31 (1988) 3532-3542.

[15] B.L. Smith, A. Glezer, The formation and evolution of synthetic jets, Phys. Fluids 10 (1998) 2281-2297.

[16] W. J. Crowther and L. T. Gomes, An evaluation of the mass and power scaling of synthetic jet actuator flow control technology for civil transport aircraft applications, Proc. IMechE. Part I: J. Syst. Control Eng. 222 (2008) 357-372.

[17] A. Vathylakis, J.H. Kim, T.P. Chong, Design of a low-noise aeroacoustic wind tunnel facility at Brunel University, Proc. 20th AIAA/CEAS Aeroacoust. Conf., AIAA 2014-3288, Atlanta, GA, 16-20 June 2014.

[18] K. Viswanathan, Instrument considerations for accurate jet noise measurements, AIAA J. 44 (2006) 1137-1149.

[19] K. K. Ahuja, Designing clean jet-noise facilities and making accurate jet-noise measurements, Intl. J. Aeroacoust. 2 (2003) 371-412.

[20] D. Arthurs, S. Ziada, Flow-excited acoustic resonances of coaxial side-branches in an annular duct, J. Fluids Struct. 25 (2009) 42-59.

[21] R. Henrywood, A. Agarwal, The aeroacoustics of a steam kettle, Phys. Fluids 25 (2013) 10710.

[22] A. Michalke, H. V. Fuchs, On turbulence and noise of an axisymmetric shear flow, J. Fluid Mechanics 70 (1975) 179-205.

[23] V. Tesar, J. Kordík, Spectral analysis of a synthetic jet, Sens. Actuators A: Phys. 167 (2011) 213-225.

[24] Y. Yang, D. L. Jones, C. Liu, Recovery of rectified signals from hot-wire/film anemometers due to flow reversal in oscillating flows, Rev. Sci. Instrum. 81 (2010) 015104.

Author Biographies

Jonne Jeyalingam is a Ph.D. candidate in the College of Engineering, Design and Physical Sciences at Brunel University London. He received his MEng degree in Aerospace Engineering at the same university in 2012. He is studying noise reduction techniques for synthetic jet actuators.

Mark Jabbal obtained his Ph.D. degree from the University of Manchester in 2008. Currently, he is Assistant Professor in the Faculty of Engineering, University of Nottingham. His research interests include all aspects of aerodynamic flow control – experimental fluid mechanics, modeling and optimization and vehicle system integration.
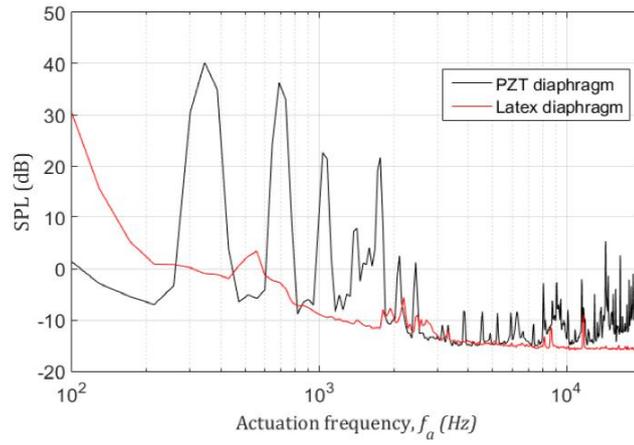
Fig. 1. Comparison of SJA diaphragm noise for PZT disc (f_a =325 Hz) and latex membrane (f_a =60 Hz)

9
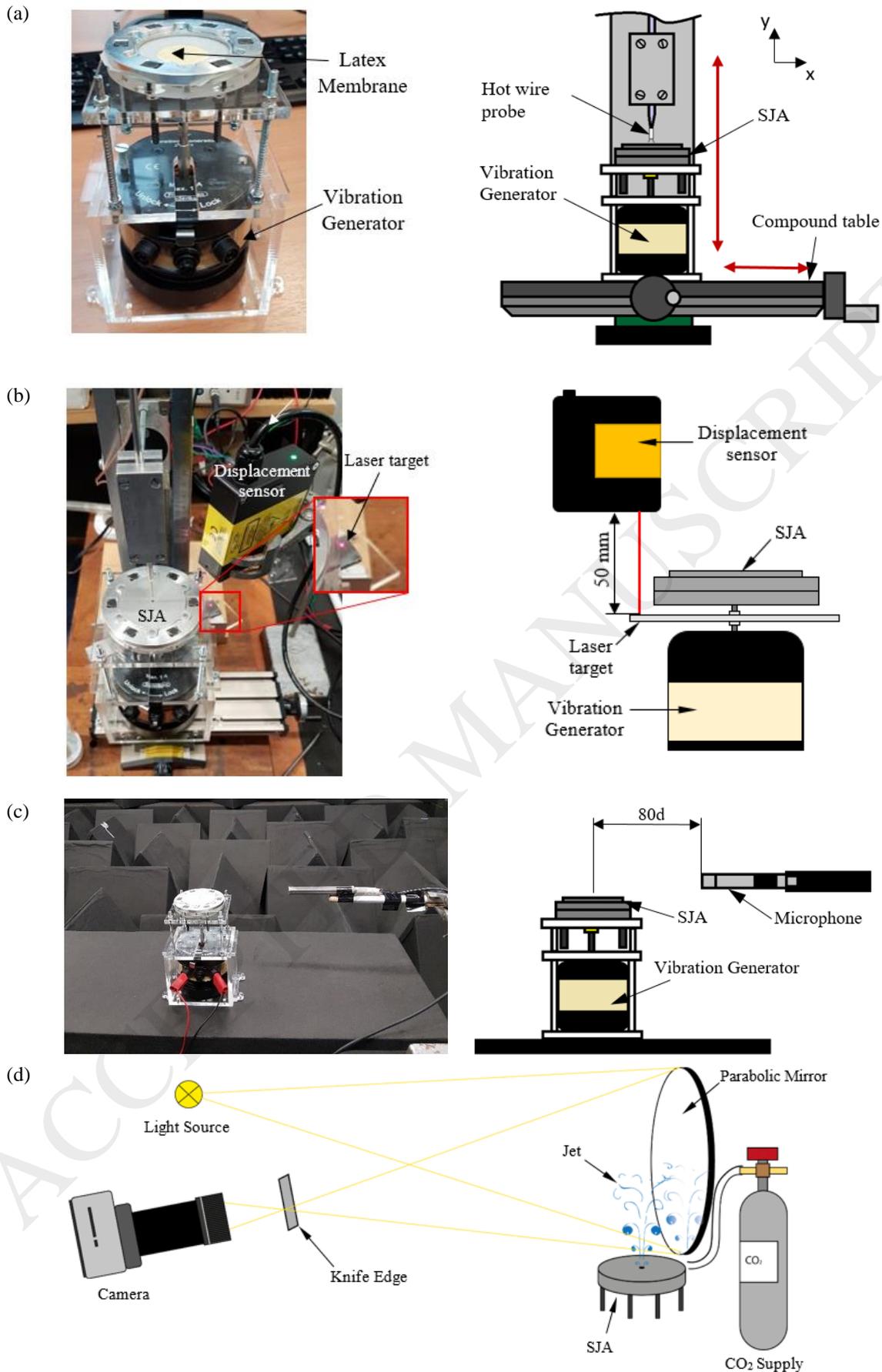
Fig. 2. SJA test set up for (a) jet velocity, (b) diaphragm displacement, (c) acoustic measurements in the anechoic chamber and (d) Schlieren visualisation

(a)

(b)
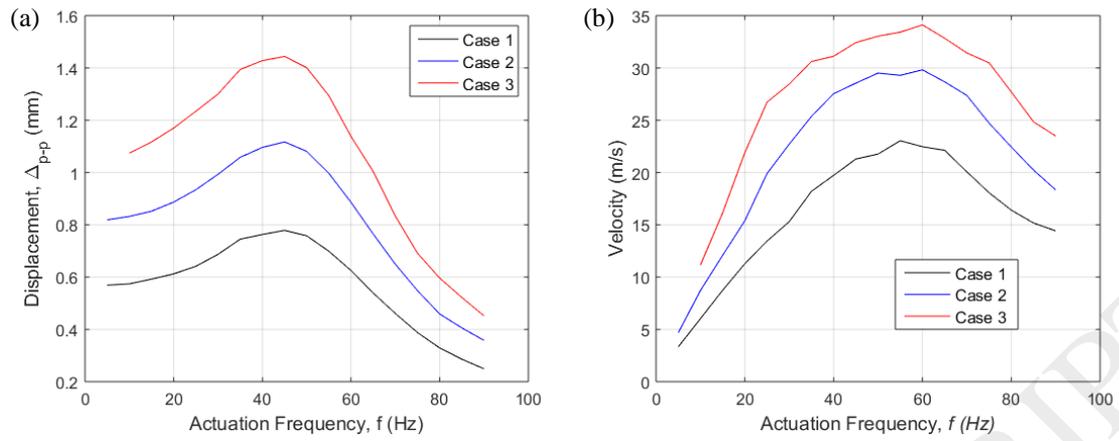
**Fig. 3. SJA frequency response (a) diaphragm peak-to-peak displacement and (b) peak jet velocity**
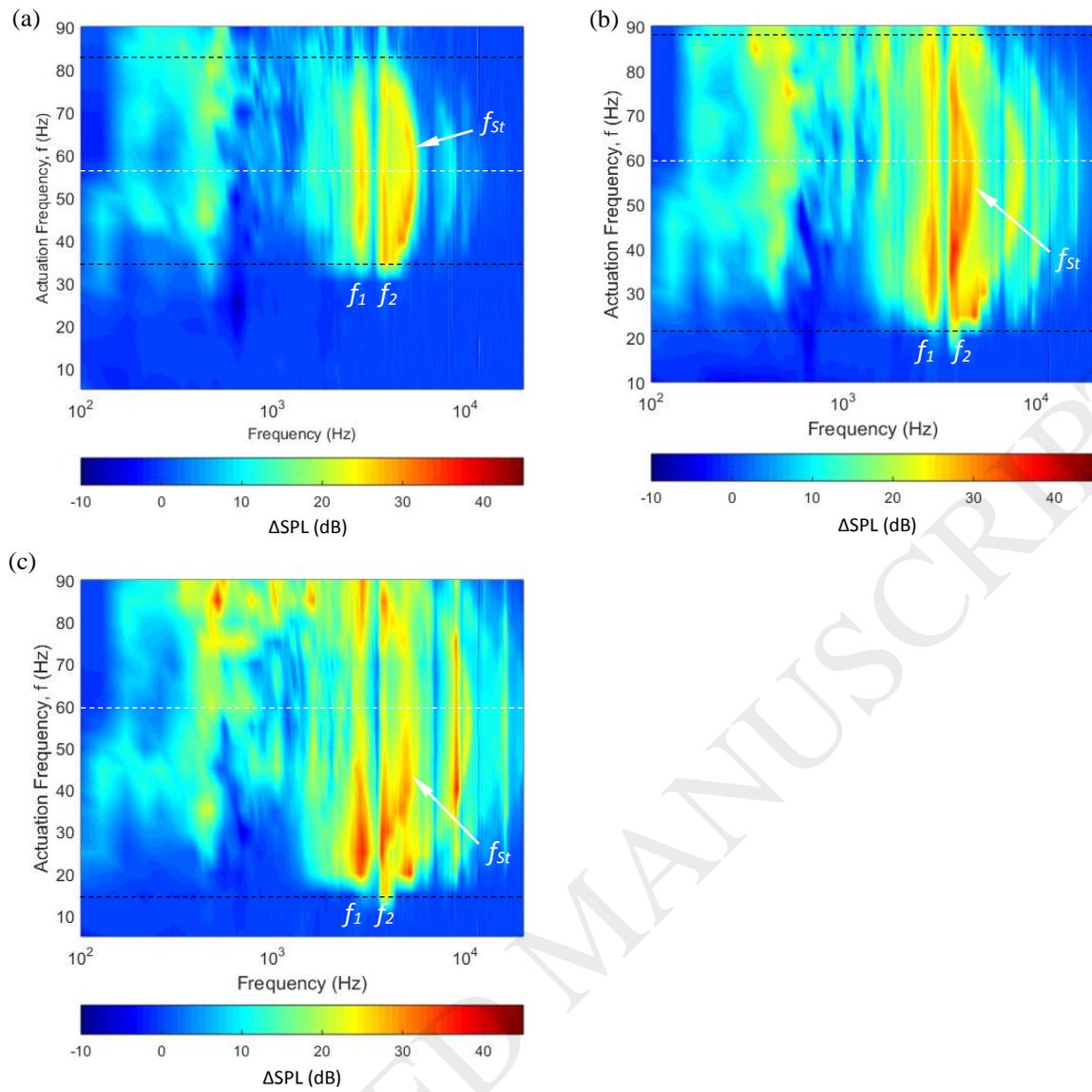
Fig. 4. SJA acoustic response (a) Case 1, (b) Case 2 and (c) Case 3. Dash black lines indicate threshold actuation frequency for whistling and dash white lines the actuation frequency for peak jet velocity

12
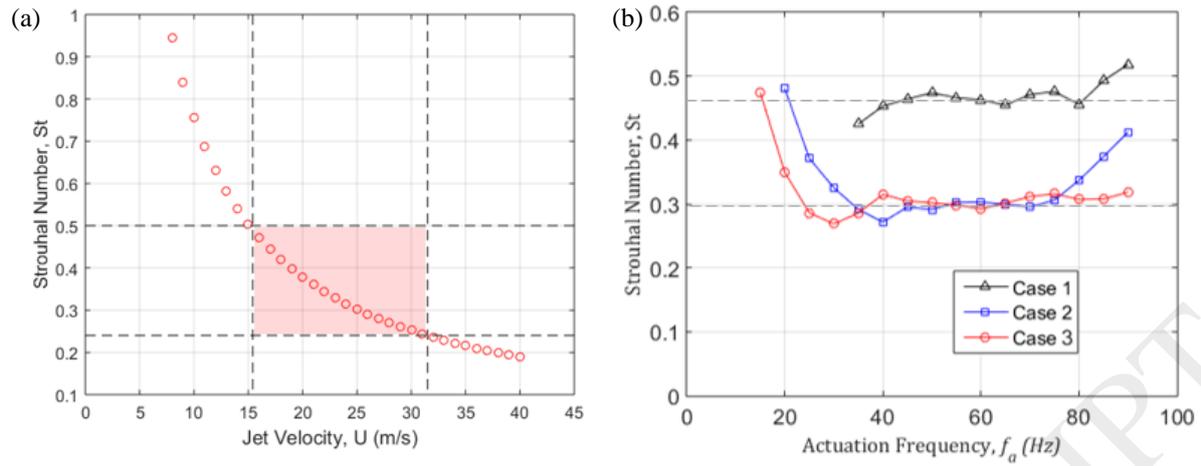
Fig. 5. Jet Strouhal number (a) as a function of jet velocity based on f_2, with range for whistling highlighted in the red region, and (b) as a function of actuation frequency based on f_{St}
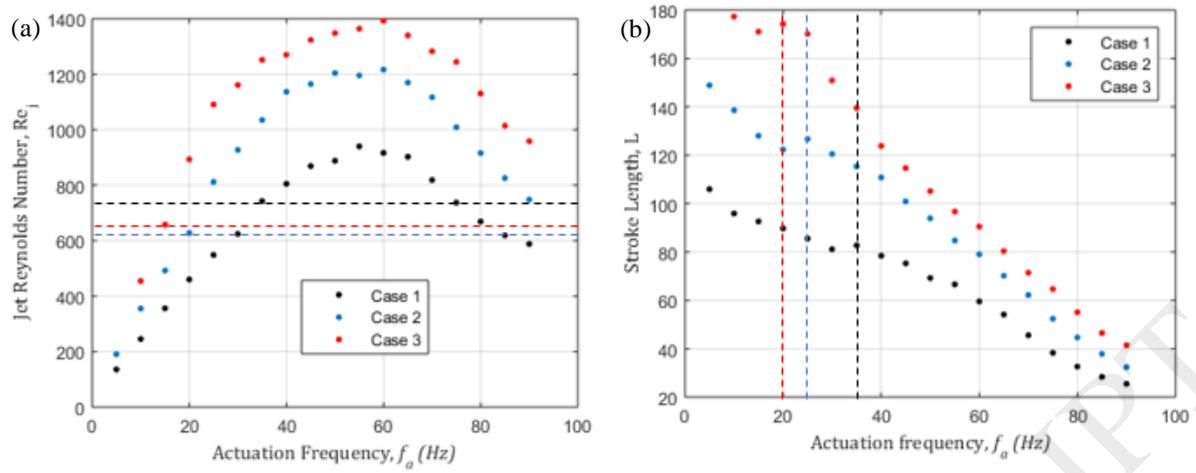
Fig. 6. Non-dimensional jet flow parameters (a) jet Reynolds number and (b) stroke length, for all three cases. Dashed lines indicate Re_j and f_a threshold respectively for the onset of whistling
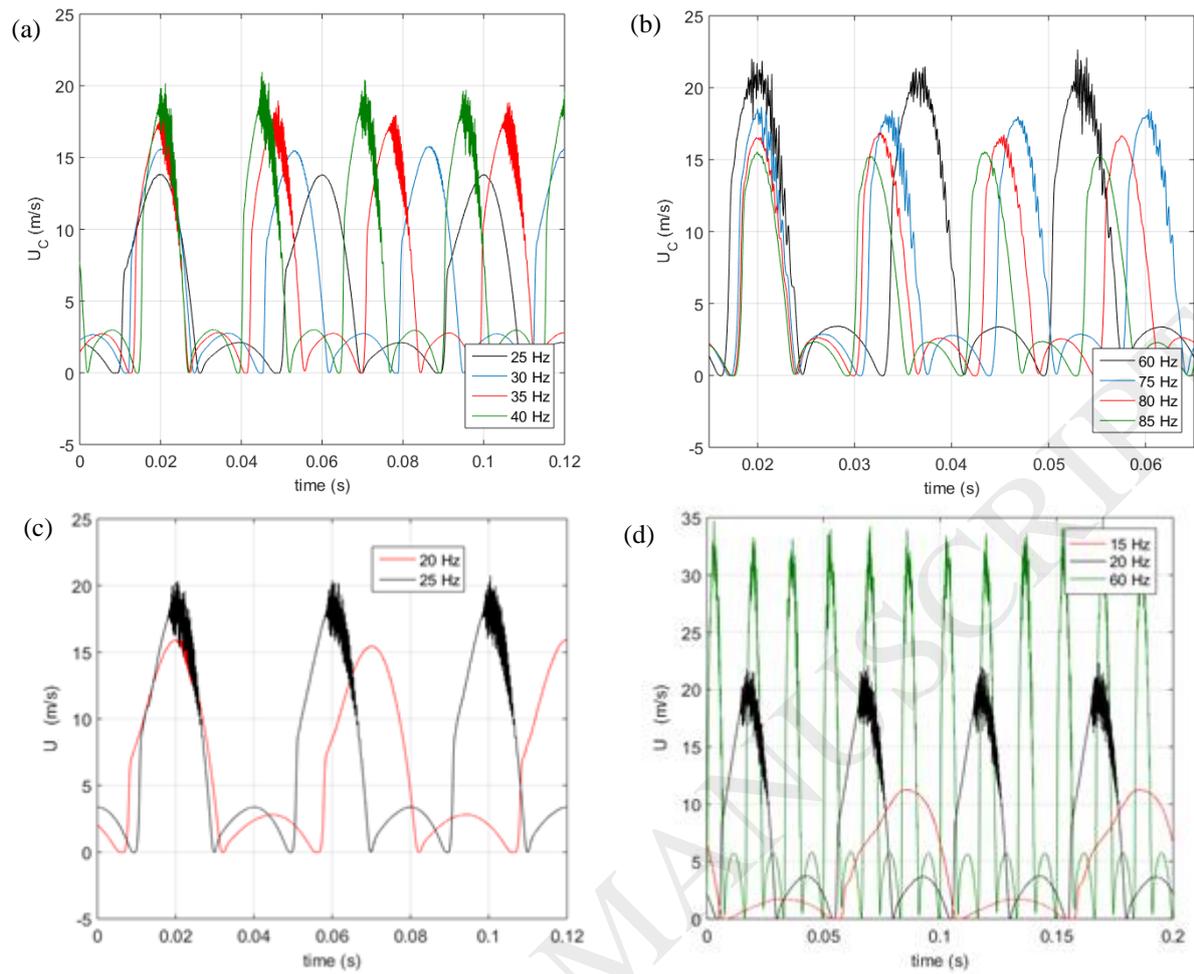
Fig. 7. Instantaneous SJA jet exit velocity response (a) Case 1: f_a 25-40 Hz, (b) Case 1: f_a 60-85 Hz, (c) Case 2, (d) Case 3.

15
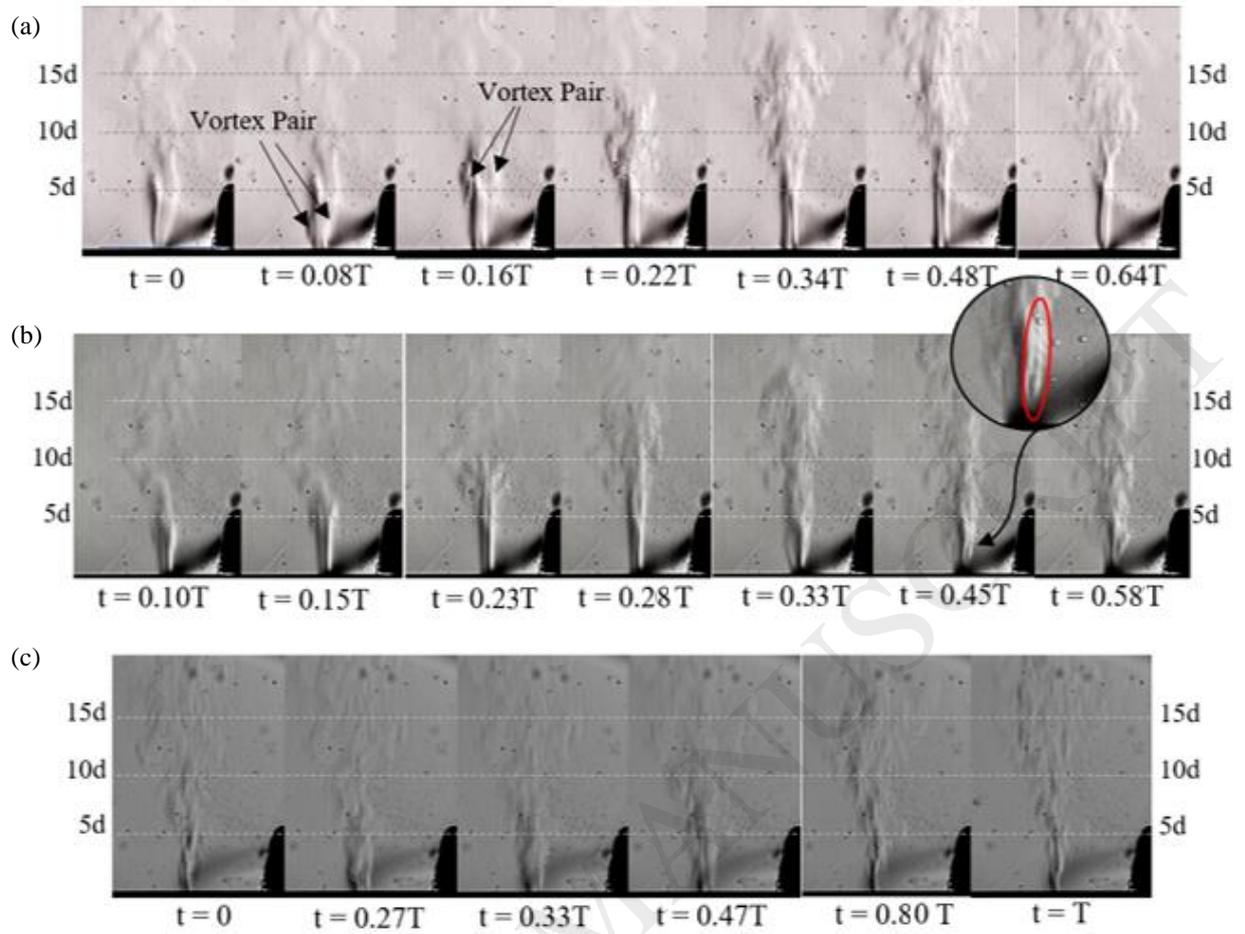
Fig. 8. Schlieren flow visualisation for Case 2 at (a) f_a = 20 Hz, (b) f_a = 25 Hz, and (c) f_a = 60 Hz.
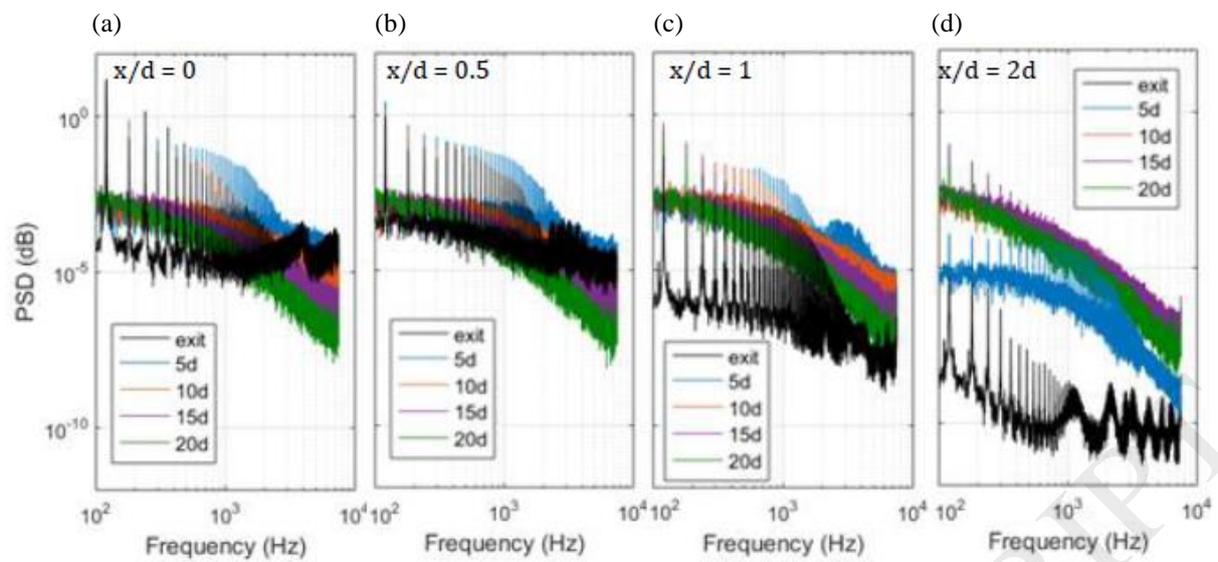
Fig. 9. Jet velocity power spectral density for Case 2, f_a = 60 Hz, as a function of five streamwise positions (exit, 5d, 10d, 15d & 20d) taken at four spanwise positions, x/d = (a) 0, (b) 0.5, (c) 1 and (d) 2
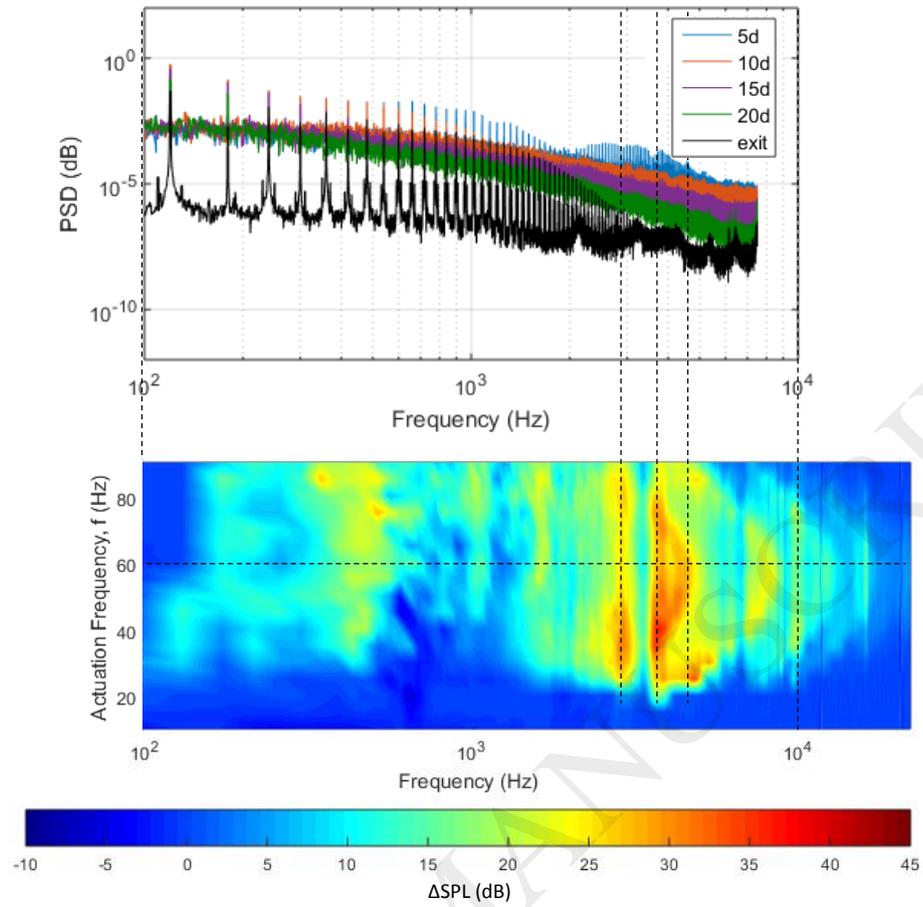
Fig. 10. Comparison of velocity spectra (upper image) and acoustic spectra (lower image) for Case 2.